PREPARATION OF Au AND Au-CARBON DOTS NANOPARTICLES WITH SESBANIA GUM AS A REDUCING AND STABILIZING REAGENT

Q. ZHANG[a*], N. ZHANG[a], X. YANG[a], H. CHEN[b], B. ZHANG[b]
*a*College of Chemistry, Tangshan Normal University, Tangshan 063000, China
*b*Hebei Chemical and Pharmaceutical Vocational Technology College,
Shijiazhuang 050026, China

Au and Au-carbon dots nanoparticles were prepared by a simple process using sesbania gum as a reducing and stabilizing agent. The morphologies, particle size distribution and optical properties of the resulting Au and Au-carbon dots nanoparticles were characterized with scanning electron microscopy, transmission electron microscopy, dynamic light scattering, ultraviolet-visible absorption spectra and fluorescent emission spectra. Effects of reaction conditions on the particle sizes and optical properties of resulting NPs were researched. Experimental results indicated that the resulting Au nanoparticles showed a relatively homogeneous and well-dispersed spherical shape, and Au-carbon dots nanoparticles exhibited a distinct core-shell structure. In addition, the mechanism for forming Au and Au-carbon dots nanoparticles was discussed.

1. Introduction

Recently, gold nanoparticles (Au NPs) have been intensively pursued as efficient drug delivery systems both in cancer diagnostics and in cancer therapy due to a combination of unique properties [1,2]. Au NPs have various attractive properties, such as good biocompatibility, low toxicity, chemical stability, strong near-infrared absorption, large surface-to-volume ratios because of their nanoscale sizes, and versatility in functionalization with various moieties including polypeptides, antibodies, DNA, protein, etc [1,3-5]. Many methods have been developed to fabricate Au NPs in which biological and chemical methods are most common. The chemical method is a simple process which controls the shape and size of the nanoparticles. Therefore, Au NPs are usually prepared by reducing chloroauric acid ($HAuCl_4$) with a variety of reducing agents, such as citrate, sodium borohydride, poly(ethylene glycols) and poly(vinyl pyrrolidone) [6-8].

Sesbania gum (SG) is an attractive biopolymer because of its abundance, low cost, non-toxic, environmentally friendly, biocompatible and biodegradable [9]. It is a kind of natural polysaccharide found in the seeds of sesbania, which grows only in China and its main structure involves β (1→4) glycosidic bonds linked mannose and α (1→6) glycosidic bonds linked galactose on the side chains. The molecular structure of SG is shown in the Fig. 1. The presence of hydroxyl groups in the structure leads to a reducing ability. The reducing ability derived from

---

*Corresponding author: zqing0703@163.com

hydroxyl groups terminated polymer have been proved by previous studies [10,11]. Therefore, Au NPs were prepared through reducing $HAuCl_4$ with SG as a reducing agent in this paper.
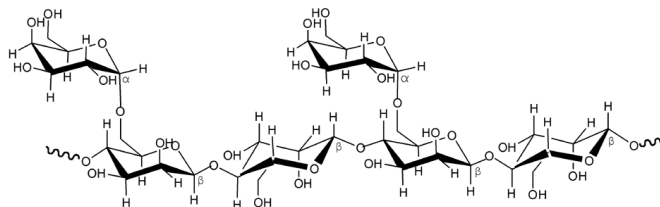
Fig. 1. Molecular structure of SG

As the new member in the family of carbon nanomaterials, carbon dots not only exhibit high fluorescence stability, photobleaching, and adjustable emission wavelength, but also have low toxicity and good biocompatibility [12-14]. Therefore, carbon dots can be used in the filed of biological fluorescence monitoring, and is expected to replace the traditional fluorescent dyes and quantum dots. In this work, the carbon dots which have abundant quaternary ammonium groups were synthesized through thermal treatment of a molecular precursor made from tris(hydroxymethyl)aminomethane and betaine hydrochloride [15]. Taking into account the advantages of both Au NPs and carbon dots, Au-carbon dots core-shell NPs were prepared through electrostatic interactions with SG as a stabilizer. To the best of our knowledge, the synthesis of Au and Au-carbon dots core-shell NPs using SG, a green and natural macromolecule compound, as the reducing agent and stabilizer has not yet been performed. Effects of reaction conditions on the particle sizes and optical properties of resulting NPs were researched. The morphologies, structure, and particle size distribution were characterized by scanning electron microscopy (SEM), transmission electron microscopy (TEM), X-ray diffractometry (XRD) and dynamic light scattering (DLS). Optical properties of the resulting nanoparticles were determined with ultraviolet-visible (UV-vis) absorption spectra and fluorescent emission spectra.

2. Experimental Methods

2.1. Materials
Sesbania gum and $HAuCl_4$ (AR) were purchased from from Zhengzhou Chengwang Chemicals Co., Ltd and Tianjin Kaima science and technology Co., Ltd, respectively. Betaine hydrochloride and tris(hydroxymethyl)aminomethane were commercially obtained from Aladdin Industrial Co., Ltd. Acetone (AR), isopropanol (AR) and sodium hydroxide (AR) were obtained from the Beijing Chemical Plant. The deionized water was generated from Milli-Q water purification system. The acetone and isopropanol were purified by distillation prior to use. Others were used as received.

2.2. Preparation of carbon dots
The carbon dots were prepared referring the literature [15]. 1.5 g betaine hydrochloride was dissolved in 5 mL of deionized water. And then, 1.2 g tris(hydroxymethyl)aminomethane was

added to the betaine hydrochloride solution until complete dissolution. The pH of mixtures was about 7. Subsequently, a soft pulp was obtained by adding an excess of isopropanol. The obtained pulp was then filtered, washed and dried for 2 days at 80 °C. The resulting viscous white mass was heated at 250 °C for 2 h in a muffle furnace, producing a brown solid. The brown solid was dissolved in 30 mL of deionized water, filtered to remove any insoluble particulates, reprecipitated through adding 150 mL acetone, and dried under the room temperature.

2.3. Preparation of Au and Au-carbon dots NPs

Au and Au-carbon dots NPs were prepared with SG as a reducing and stabilizing reagent, respectively. SG was first purified by dissolving, centrifugation and drying treatments. 0.5 g of purified SG was dissolved in 60 mL of deionized water. Then 30 mL of aqueous solution of $HAuCl_4$ were added into the SG aqueous solution. The mixtures were heated at a certain temperature and pH under mechanical stirring for 3h, resulting in the formation of Au NPs.

0.0340g of carbon dots was dissolved in 60 mL deionized water, followed by adding an appropriate amount of Au nano-colloidal solutions. The Au NPs were reacted with carbon dots at pH between 8 and 12 and the mixture was stirred for 2 h with a homogenizer under 60 °C. Subsequently, the resulting mixture was separated by centrifugation, washed with deionized water and re-suspended in water.

2.4. Characterization

The morphology and structure of the nanoparticles were characterized with a Sigma300 SEM and a JEM-2010 TEM, respectively. The samples for SEM were dried on adhesive carbon disks, and the samples forTEM were prepared by sonicating the nanoparticle dispersions and then depositing a drop onto a carboncoated grid, which was allowed to dry in air. The particle size distribution was measured by a ZetaPlus Zeta Potential Analyzer (ZZPA). The XRD pattern was collected in reflection geometry using a Rigaku RINT2000 X-ray diffractometer at room temperature with Cu Ka radiation. The UV-vis absorption spectra and fluorescence emission spectra of core-shell nanoparticles were analyzed with a UV- 2450 UV-visible spectrophotometer and a PerkinElmer LS 55 spectrofluorometer, respectively.

3. Results and discussion

3.1. Au NPs
3.1.1 Morphologies and particle size distribution
Fig. 2a displays the TEM micrograph of Au NPs. From the micrograph, one can see that the resulting Au NPs show a relatively homogeneous and well-dispersed spherical shape. The average particle size of the particles estimated by measuring the diameter of approximately 100 randomly selected NPs in TEM images is about 36.8 nm, and the corresponding standard deviation is 1.8 nm.
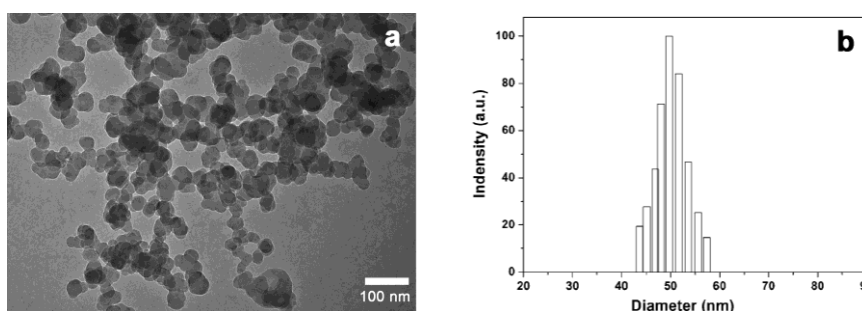
Fig. 2. (a) TEM micrograph and (b) particle size distribution of Au microspheres prepared with 1×10^{-3} mol/L HAuCl$_4$ aqueous solution

The result of DLS (Fig. 2b) shows that the particle sizes of nanoparticles are in the range of 43-57 nm. Compared to the results of TEM, the size of the particles measured by DLS is larger. The reason is the DLS measurement includes the contribution of the SG molecule extended in the solution, which shows no contrast in the TEM study [16]. In addition, the shrinking of the particles caused by electron beam damage is also an explanation for the size differences measured by TEM and DLS.

Table 1. Average particle sizes and area densities of Au NPs obtained with varying concentrations of HAuCl$_4$

C_{HAuCl_4} /mol/L	Average particle size /nm	Area density /m^{-2}
1×10^{-4}	36.2 ± 1.6	0.6×10^8
5×10^{-4}	36.3 ± 1.5	2.5×10^8
1×10^{-3}	36.8 ± 1.8	5.9×10^8
5×10^{-3}	47.1 ± 2.4	8.6×10^8
1×10^{-2}	61.0 ± 3.1	1.1×10^9
5×10^{-2}	83.5 ± 5.2	1.2×10^9

The concentration of HAuCl$_4$ aqueous solution played an important role in controlling the particle size. The influence of HAuCl$_4$ solution concentration was researched within the range of $1\times10^{-4}\sim5\times10^{-2}$ mol/L, whereas all the other reaction parameters were held constant. The average particle sizes and area densities were calculated with the ImageJ software, and the results were listed in Table 1. It was found that with an increase in the concentration of HAuCl$_4$, both average particle sizes and area densities of Au NPs increased. When the concentration of HAuCl$_4$ increased to 5×10^{-2} mol/L, the average particle sizes and area densities were the largest among the samples at 83.5 ± 5.2 nm and 1.5×109 m^{-2}, respectively. The large particle sizes could be attributed to the agglomeration between nanoparticles, which was in agreement with the previous reports by Abedini et al. [17,18], who prepared various sizes of metallic nanoparticles through tuning reaction conditions and concluded that too high concentration of HAuCl$_4$ solution resulted in the aggregation of Au NPs. In addition, a negligible increase of average particle size (36.2 ± 1.6 and

36.3±1.5 nm) was seen as the concentration was below 1×10^{-3} mol/L, although there was an obvious rise in the area density.

3.1.2 Optical properties

SG was employed as a reducing reagent to prepare Au NPs in the present work. When HAuCl$_4$ was added in SG solution, SG slowly deoxygenized Au (III) into Au (0) at a certain reaction condition. And the color of the mixture gradually changed from transparent to purple. Fig. 3 shows the UV-vis spectrum of the reaction mixture after the reaction takes place. In the Fig. 3 a well-defined absorption peak was observed at 525 nm, which was attributed to the typical absorption band of Au NPs due to the surface plasmon resonances. This was in coincidence with the reported plasmon resonance absorption peak of AuNPs [19], indicating the successful preparation of Au NPs.
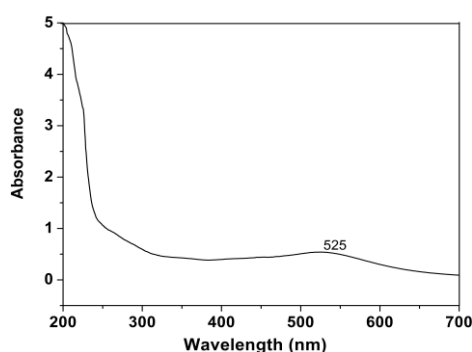
Fig. 3. UV-vis spectrum of the reaction mixture after the reaction took place.

The influence of the reaction temperature was researched within the range of 40~90 ^{o}C. Fig. 4 shows UV-vis spectra and photos of the resulting Au NPs under the different temperature, respectively. It was found that the maximum absorption peak of Au NPs was first blue-shifted from 529 to 525 nm with the increase of the reaction temperature from 40 to 70 ^{o}C, and then red-shifted gradually. The blue-shift and red-shifted were attributed to the decrease and increase in the particle size of nanoparticles, respectively. Therefore, we concluded that as the temperature increases, the particle size of the resulting Au NPs decreases first and then increases. The reason may be that the reaction rate was accelerated with the increase of temperature, which led to the faster nucleation of the nanoparticles, resulting in smaller particles. However, when the temperature reached to a certain value, the aggregation between particles occurred and thus formed the larger particles. In addition, as the reaction temperature was ranged from 40 to 90 ^{o}C, the color of the dispersions of Au NPs was gradually deepened (Fig. 4 inset), which indicated that the amount of Au NPs obtained increased.
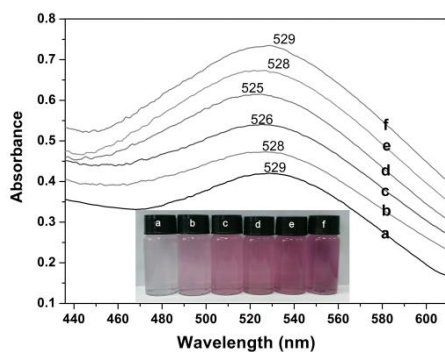
Fig. 4. UV-vis spectra and photographs (the inset) of the resulting Au NPs under the different temperature: (a) 40 ^{o}C, (b) 50 ^{o}C, (c) 60 ^{o}C, (d) 70 ^{o}C, (e) 80 ^{o}C and (f) 90 ^{o}C.

3.1.3. XRD analysis

The structure of Au NPs was further confirmed by the XRD analysis. Fig. 5 shows the XRD pattern of Au NPs. The standard pattern of Au (JCPDS no. 04-0784) was shown as a reference.
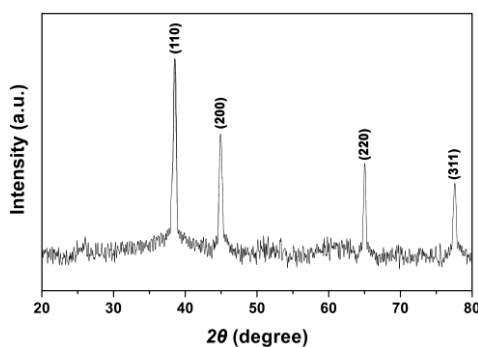
Fig. 5. XRD pattern of Au NPs.

As seen in Fig. 5, Bragg peaks of Au are observed, and Au NPs exhibit four sharp diffraction peaks at 2θ of 38.4^{o}, 44.8^{o}, 65.1^{o}, and 77.9^{o}, which are attributed to the (111), (200), (220) and (311) planes of the face-centered cubic structure, respectively. This was in good agreement with the standard pattern. All these observations indicate that the Au NPs have been successfully prepared by the reduction of HAuCl$_4$ using SG as the reducing agent.

3.2. Au-carbon dots NPs
3.2.1. Morphologies and particle size distribution

Core-shell nanoparticles with Au as the core and carbon dots as the shell were prepared through the electrostatic interactions using SG as the stabilizing agent. Fig. 6a-c shows the SEM micrograph, TEM micrograph, and particle size distribution of Au-carbon dots NPs. As can be seen from the micrographs in Fig. 6a and b, the resulting Au-carbon dots NPs exhibit well-dispersed spherical shapes, and represent clear core-shell structures. Evidently, the Au NPs are covered with the smaller carbon dots. Since the individual Au NP consisted of a large number of carbon dots, the surface of the Au-carbon dots NPs is very rough. The average particle size of

the particles calculated from TEM is approximately 89.5 nm, and the corresponding standard deviation is 3.2 nm. Bimodal size distribution is observed, as shown in the result of DLS (Fig. 6c), which indicates the coexistence of both large and small Au-carbon dots NPs. The sizes of the majority of particles are in the range of 105-118 nm, but a few particles above 130 nm are found.
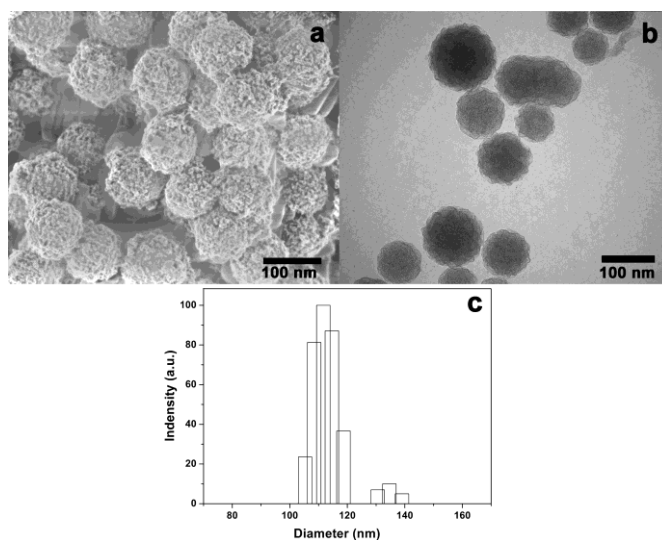
Fig. 6. (a) SEM micrograph, (b) TEM micrograph, and (c) Particle size distribution of Au-carbon dots NPs.

3.2.2. Optical properties

The absorption-emission spectra of Au-carbon dots NPs are shown in Fig. 7. One could see from Fig. 7a, the characteristic absorption peak located at 360 nm was attributed to the n-π* transition in the C=O bond [20,21]. The C=O bond was derived from amide groups which decorated on the surface of carbon dots. Fig. 7b revealed a characteristic strong and narrow emission peak centered at 434 nm under an excitation wavelength of 360 nm. And the Au-carbon dots NPs exhibited strong blue luminescence under excitation at 365 nm with a UV lamp (Fig. 7 inset).
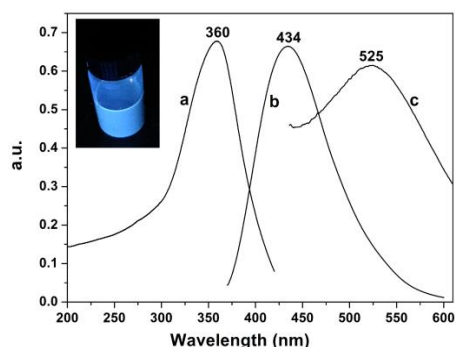
Fig. 7. Absorption (a) and emission (b) spectra of Au-carbon dots NPs, and absorption absorption spectrum of Au Nps (c). The inset is a digital photograph of Au-carbon dots NPs under UV light (365 nm).

It was found in Fig. 7(c), partial overlap occurred between the fluorescence emission spectrum of Au-carbon NPs and the UV-visible absorption spectrum of Au NPs. Therefore, It can be concluded that an energy transfer process could takes place in the Au-carbon dots NPs system, and carbon dots and Au NPs acts as donors and receptors, respectively. Since the emission of fluorescence from carbon dots took place during the recombination of excited electron with the ground state, and the energy receptors (Au NPs) prevented the recombination of charge carriers. This may lead to fluorescence quenching effect, which was displayed at reduced fluorescence intensity. Fig. 8 shows the fluorescence emission spectra of carbon Au-carbon dots NPs obtained under the different amounts of Au NPs. One could see that with an increase in the amount of Au NPs, the fluorescence intensity of Au-Carbon dots NPs gradually weakened, indicating an efficient quenching process.
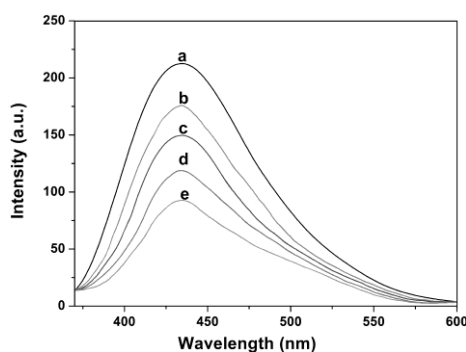
Fig. 8. Fluorescence emission spectra of carbon Au-carbon dots NPs prepared under the different amounts of Au NPs (obtained with 1×10^{-3} mol/L $HAuCl_4$ solution): (a) 5.5 mL, (b) 6.5 mL, (c) 7.5 mL, (d) 8.5 mL and (e) 9.5 mL

In addition, the fluorescence intensity of aqueous dispersions of Au-carbon dots NPs with a constant concentration of Au NPs was investigated for heating at 100 °C for the periods from 24 to 168 h. It was found that the fluorescence intensity almost remained stable, which indicated that the above quenching was probably static in nature, and the Au-carbon dots NPs could keep the long-range fluorescence stability.

3.3 Mechanism for the formation of Au and Au-carbon dots NPs

SG was used as a reducing and stabilizing reagent to prepare Au and Au-carbon dots NPs in this paper. The surface of SG molecule was rich in hydroxyl groups, which could reduce Au (III) into Au (0) and the hydroxyl groups were transformed into carbonyl groups. The reducing ability of SG was derived from hydroxyl groups [10]. Besides, a stabilizing reagent plays an important role in preventing nanoparticles from aggregating. In the present work, only SG was mixed with $HAuCl_4$, and the obtained Au NPs had a relatively homogeneous and well-dispersed spherical shape. This may be because that hydrogen bonding formed between hydroxyl groups of SG surface that were not oxidized and Au NPs, and SG molecules were attached to the surface of Au NPs. Therefore, the resulting Au NPs were stable and did not aggregate at a certain reaction conditions.

The carbon dots NPs obtained by the method of Bourlinos et al. were decorated with quaternary ammonium groups (i.e., $-N(CH_3)^{3+}$) derived from the betaine ligand, which allowed them to be immobilized on an anionic substrate by electrostatic interactions [15]. The surface of the resulting Au NPs was attached by SG molecules, so the hydroxyl groups that were not

oxidized by Au(III) were converted to oxygen anions (i.e., SG–OH→SG–O$^-$ + H$^+$) at a pH of 8~12. Therefore, Au-carbon dots core-shell nanoparticles were formed by electrostatic interactions between the positively charged carbon dots and the negatively charged Au NPs. The schematic diagram was shown in Fig. 9.
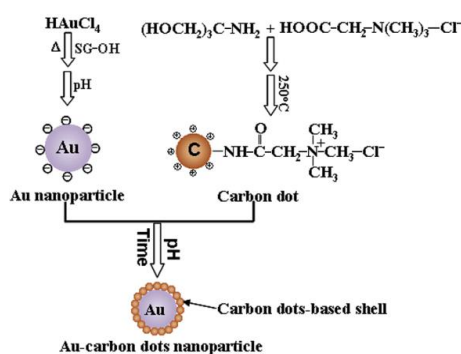
Fig. 9. Schematic diagram for preparing Au and Au-carbon dots NPs.

4. Conclusions

In summary, we synthesized Au NPs by the reduction of HAuCl$_4$ using SG as the reducing agent, and Au-carbon dots core-shell NPs through electrostatic interactions with SG as the stabilizer. The morphologies, structure, particle size distribution and optical properties of the resulting nanoparticles were characterized. Experimental results indicated that the resulting Au NPs showed a relatively homogeneous and well-dispersed spherical shape, and Au-carbon dots NPs exhibited a distinct core-shell structure.

With an increase in the concentration of HAuCl$_4$, both average particle sizes and area densities of Au NPs increased. As the temperature increases, the maximum absorption peak of Au NPs was first blue-shifted and then red-shifted. Moreover, Au-carbon dots NPs exhibited an efficient quenching process with an increase in the amount of Au NPs used during the preparation. In addition, the mechanism for forming Au and Au-carbon dots NPs was discussed. The present work will provide a new idea and theoretical basis for the application of multifunctional nanocomposites in the targeted therapy and monitoring of cancer cells.

References

[1] S. Rajkumar, M. Prabaharan, Current Topics in Medicinal Chemistry **17**(16), 1858 (2017).
[2] P. Chandra, D. Das, A. A. Abdelwahab, Digest Journal of Nanomaterials and Biostructures **5**(2), 363 (2010).
[3] Y. Ohmi, S. Nishimura, K. Ebitani, *ChemSusChem*, **6**, 2259 (2013).

[4] T. Isogai, A. Piednoir, E. Akada, Y. Akahoshi, R. Tero, S. Harada, T. Ujihara, M. Tagawa, Journal of Crystal Growth **401**(9), 494 (2014).

[5] D. Cabuzu, A. Cirja, R. Puiu, A. M. Grumezescu, Current Topics in Medicinal Chemistry **15**(16), 1605 (2015).

[6] H. du Toit, T. J. Macdonald, H. Huang, I. P. Parkinb, A. Gavriilidis, RSC Advances **7**, 9632 (2017).

[7] B. Yang, J. Chou, X. Dong, C. Qu, Q. Yu, K. J. Lee, N. Harvey, The Journal of Physical Chemistry C **121**, 8961 (2017).

[8] A. Sobczak-Kupiec, D. Malina, M. Zimowska, Z. Wzorek, Digest Journal of Nanomaterials and Biostructures **6**(2), 803 (2011).

[9] Q. Zhang, Y. Gao, Y. A. Zhai, F. Q. Liu, G. Gao, Carbohydrate Polymers **73**, 359 (2008).

[10] X. Wang, Y. Long, Q. Wang, H. Zhang, X. Huang, R. Zhu, P. Teng, L. Liang, H. Zheng, carbon **64**, 499 (2013).

[11] I. Washio, Y. J. Xiong, Y. D. Yin, Y. N. Xia, Advanced Materials **18**(13), 1745 (2006).

[12] J. Hou, J. Dong, H. Zhu, X. Teng, S. Ai, M. Mang, Biosensors and Bioelectronics **68**, 20 (2015).

[13] J. Peng, W. Gao, B. K. Gupta, Z. Liu, R. Romero-Aburto, L. Ge, L. Song, L. B. Alemany, X. Zhan, G. Gao, S. A. Vithayathil, B. A. Kaipparettu, A. A. Marti, T. Hayashi, J. J. Zhu, P. M. Ajayan, Nano Letters**12**(2), 844 (2012).

[14] S. Zhu, Q. Meng, L. Wang, J. Zhang, Y. Song, H. Jin, K. Zhang, H. Sun, H. Wang, B. Yang, Angewandte Chemie International Edition **52**(14), 3953 (2013).

[15] A. B. Bourlinos, R. Z., J. Petr, A. Bakandritsos, M. Krysmann, E. P. Giannelis, Chemistry of Materials **24**, 6 (2012).

[16] Q. Zhang, Nano **9**(3), 1450028 (2014).

[17] A. Abedini, A. R. Daud, M. A. A. Hamid, N. K. Othman, E. Saion, Nanoscale Research Letters **8**, 1 (2013).

[18] S. A. Ng, K. A. Razak, K. Y. Cheong, K. C. Aw, Thin Solid Films **615**, 84 (2016).

[19] W. Byoun, H. Yoo, ChemistrySelect **2**, 2414 (2017).

[20] S. S. Liu, C. F. Wang, C. X. Li, J. Wang, L. H. Mao, S. Chen, Journal of Materials Chemistry C **2**(32), 6477 (2014).

[21] Y. Zhang, J. Zhang, J. Zhang, S. Lin, Y. Huang, R. Yuan, X. Liang, W. Xiang, Dyes Pigments **140**, 122 (2017).